

# X-ray polarisation signatures in bombarded magnetar atmospheres

Ruth M. E. Kelly,<sup>1\*</sup> Denis González-Caniulef,<sup>2</sup> Silvia Zane,<sup>1</sup> Roberto Turolla<sup>1,3</sup> and Roberto Taverna<sup>3</sup>

<sup>1</sup>Mullard Space Science Laboratory, University College London, Holmbury St Mary, Dorking, Surrey RH5 6NT

<sup>2</sup>Institut de Recherche en Astrophysique et Planétologie, 9 avenue du Colonel Roche, BP 44346 31028, Toulouse CEDEX 4, France

<sup>3</sup>Università di Padova, Dipartimento di Fisica e Astronomia, via Marzolo 8, I-35131 Padova, Italy

Accepted XXX. Received YYY; in original form ZZZ

## ABSTRACT

Magnetars are neutron stars that host huge, complex magnetic fields which require supporting currents to flow along the closed field lines. This makes magnetar atmospheres different from those of passively cooling neutron stars because of the heat deposited by backflowing charges impinging on the star surface layers. This particle bombardment is expected to imprint the spectral and, even more, the polarisation properties of the emitted thermal radiation. We present solutions for the radiative transfer problem for bombarded plane-parallel atmospheres in the high magnetic field regime. The temperature profile is assumed a priori, and selected in such a way to reflect the varying rate of energy deposition in the slab (from the impinging currents and/or from the cooling crust). We find that thermal X-ray emission powered entirely by the energy released in the atmosphere by the magnetospheric back-bombardment is linearly polarised and X-mode dominated, but its polarisation degree is significantly reduced (down to 10%–50%) when compared with that expected from a standard atmosphere heated only from the cooling crust below. By increasing the fraction of heat flowing in from the crust the polarisation degree of the emergent radiation increases, first at higher energies ( $\sim 10$  keV) and then in the entire soft X-ray band. We use our models inside a ray-tracing code to derive the expected emission properties as measured by a distant observer and compare our results with recent *IXPE* observations of magnetar sources.

**Key words:** polarisation – radiative transfer – stars: atmospheres – stars: magnetars

## 1 INTRODUCTION

Powered by their own magnetic energy, soft  $\gamma$ -repeaters (SGRs) and anomalous X-ray pulsars (AXPs) are two groups of isolated neutron stars which together make up the class known as magnetars (Duncan & Thompson 1992; Thompson & Duncan 1993). They are typically characterised by persistent X-ray luminosities  $L \approx 10^{31}$ – $10^{36}$  erg s<sup>−1</sup>, spin periods  $P \sim 1$ –12 s (with the exception of the transient source 3XMM J185246.6+003317, that has been proposed to have a period of 23 s, see Hambaryan et al. 2015) and exhibit period derivatives  $\dot{P} \sim 10^{-13}$ – $10^{-10}$  s s<sup>−1</sup>, from which ultra strong magnetic fields  $B \sim 10^{13}$ – $10^{15}$  G can be inferred.

Magnetars are expected to have internal magnetic fields more complex than a pure dipole, with both a poloidal and a toroidal component. The stresses exerted on the crust by the latter induce the formation of local twists in the external magnetic field, which becomes non-potential and needs to be supported by currents flowing along the closed field lines. Photons emitted from the cooling surface undergo repeated resonant Compton scatterings (RCSs) with the moving particles, producing a thermal+power-law spectrum in agreement with observations (the RCS paradigm; Thompson et al. 2002, see also Turolla et al. 2015).

Due to the strength of the magnetic field, magnetar emission is expected to be linearly polarised in two normal modes, referred to as the ordinary (O), with electric field vector oscillating in the plane

of the propagation direction and the local magnetic field, and the extraordinary (X) one, with the electric vector oscillating perpendicular to the same plane. The large difference in the opacities, which are much lower for the X-mode, is at the basis of the expected large polarisation of radiation coming from a strongly magnetised plasma (see e.g. Harding & Lai 2006; Potekhin et al. 2017; González Caniulef et al. 2016). Additionally, vacuum also contributes to shape the optical properties of the medium. This results in the occurrence of vacuum birefringence and the appearance of the vacuum resonance, where the polarisation modes may switch (Adler 1971; Lai & Ho 2003; Ho & Lai 2003). Both these effects strongly influence the polarisation of radiation as measured at infinity.

Imaging X-ray Polarimetry Explorer (*IXPE*; Weisskopf et al. 2022), a joint NASA-ASI space mission and the first telescope devoted to a systematic study of the sky in polarised X-rays, has observed four magnetars to date; the AXPs 4U 0142+61 (Taverna et al. 2022), 1RXS J170849.0–400910 (hereafter 1RXS J1708 for short, Zane et al. 2023) and 1E 2259+586 (Heyl et al. 2024), and the SGR 1806–20 (Turolla et al. 2023). Polarisation has been detected for all the sources, albeit to different levels of confidence (see also Taverna & Turolla 2024, for a review).

Both 4U 0142+61 and 1RXS J1708 show polarisation properties which are highly energy dependent. 1RXS J1708 was found to have a constant polarisation angle while the polarisation degree increases from  $\approx 20\%$  at 2–3 keV to  $\approx 80\%$  at 6–8 keV (Zane et al. 2023). On the other hand, 4U 0142+61 exhibits a polarisation degree of  $\approx 15\%$  at 2–4 keV and  $\approx 35\%$  at 6–8 keV, dropping to zero at 4–5 keV

\* E-mail: ruth.kelly.22@ucl.ac.uk

where the polarisation angle swings by  $90^\circ$ , indicating a switch of the dominant polarisation mode from low to high energies (Taverna et al. 2022). Only a marginally significant polarisation degree of  $31.6 \pm 10.5\%$  was detected in the 4–5 keV range for SGR 1806–20, with  $3\sigma$  upper limits of 24% and 55% in the 2–4 and 5–8 keV bands, respectively (Turolla et al. 2023). 1E 2259+586 was found to have a mild, phase-dependent polarisation degree, ranging from  $\approx 0$  to  $\approx 25\%$  (Heyl et al. 2024).

The polarisation properties from both 4U 0142+61 and SGR 1806–20 can be explained by the reprocessing of thermal radiation from a condensed surface by RCS in the star twisted magnetosphere (Taverna et al. 2020, 2022; Turolla et al. 2023). The polarisation signature of 1RXS J1708 is, instead, compatible with thermal emission coming from two regions of the surface, one covered by a standard atmosphere, the other in a magnetically-condensed state (Zane et al. 2023). An alternative model has been proposed by Lai (2023), according to which the polarisation pattern of 4U 0142+61 and 1RXS J1708 could be due to partial mode conversion at the vacuum resonance in the star atmosphere. A recent, more comprehensive study of atmospheres with partial mode conversion, however, questions this result (Kelly et al. 2024). Finally, a baryon-loaded magnetic loop (similar to that proposed for SGR 0418+5729 by Tiengo et al. 2013) can explain the phase-dependent absorption line and polarisation properties of 1E 2259+586 (Heyl et al. 2024).

The suggestion that the low-energy spectral components observed by *IXPE* originate in the solid crust was put forward mainly to explain two features: a) the relatively modest polarisation, and b) the fact that they appear to be polarised either in the O mode (as in 4U 0142+61 and 1E 2259+586) or in the X mode (as in 1RXS J1708). These two facts are difficult to explain with standard atmospheric emission from a passive cooler. However, it is possible that atmospheric models computed under different assumptions provide an alternative, viable interpretation to the solid surface scenario. For instance, atmospheres around active magnetars are expected to be at variance with those of other (strongly) magnetised NSs, inasmuch the magnetospheric currents (needed to sustain the twisted field) impact on the star outer layers, depositing heat, a phenomenon known in literature as “particle bombardment”. It has been proposed (see e.g. González-Caniulef et al. 2019; Mushtukov et al. 2021; Taverna et al. 2022; Taverna & Turolla 2024) that the extra heat deposited in the external surface layers may produce a) a substantial reduction in the polarisation of the emergent radiation, and b) inner atmospheric layers characterised by an “inverted temperature profile” (with the temperature decreasing at larger depths), which, in turn, can give rise to O-dominated emergent radiation (see § 2). A self-consistent modelling of magnetar atmospheres, accounting for the bombardment effect, is therefore warranted to investigate this possibility and confront spectro-polarimetric data.

An initial investigation into this effect has been carried out by González-Caniulef et al. (2019) who studied the problem of the thermal structure of a gray, bombarded atmosphere. In this work we expand upon these first results, exploring to what extent particle bombardment influences the frequency dependent properties of thermal radiation emitted by the atmosphere.

The paper is laid out as follows. In section 2 we review the basic characteristics of the expected atmospheric temperature profile under different assumptions, the physics of heat deposition by particle bombardment, the atmospheric model calculations and the assumptions made throughout our investigation. We present our numerical results in section 3 and compare our findings with observed polarisation signatures in section 4. Finally, discussion and conclusions are presented in section 5.

## 2 THEORETICAL BACKGROUND

### 2.1 Atmospheric temperature profile

The aim of this paper is to study the propagation of radiation in a magnetised NS atmosphere accounting for different temperature profiles, with a focus on how the temperature gradient affects the polarisation signal. We do not self-consistently solve the energy balance and radiation field, since this would require the development of a new numerical code, which is beyond the scope of the present work. The temperature run, instead, is specified a priori, starting from the results obtained in previous investigations on both passive and bombarded atmospheres. For the sake of completeness, these are reviewed below.

A passively cooling neutron star, for which only the release of internal heat is responsible for the thermal emission, can be assumed to be covered by an atmosphere that is in local thermodynamic, radiative and hydrostatic equilibrium. Under these assumptions, atmospheric models have been computed by several authors (see e.g. Hernquist 1985; Romani 1987; Pavlov et al. 1996; Ho & Lai 2001). The energy balance equation can be expressed in the form

$$\chi_p \left[ \frac{aT^4}{2} - \frac{\chi_p^{(1)} U^{(1)}}{\chi_p} - \frac{\chi_p^{(2)} U^{(2)}}{\chi_p} \right] = 0, \quad (1)$$

where,  $\chi_p^{(j)}$  and  $U^{(j)}$  are the Planck mean opacity and the energy density, respectively, referred to the normal mode  $j$  (here  $j = 1$  is the extraordinary, X, and  $j = 2$  is the ordinary, O, one), while  $\chi_p$  is the total Planck mean opacity. The basic feature of the resulting temperature profile is that it increases monotonically with increasing depth. Due to different frequencies decoupling at different temperatures, this profile produces a typical hardening in the spectrum. Owing to the lower opacity, the X-mode decouples at higher temperatures and is therefore expected to dominate the emergent radiation signal (Pavlov et al. 1994; Harding & Lai 2006; Potekhin 2014).

As stated above, the situation can be quite different in the case of magnetars, since returning currents may provide another source of heat, which is deposited as the back-flowing charges hit the atmosphere. This effect has been discussed by González-Caniulef et al. (2019) in the low-density plasma regime. Specifically, these authors computed frequency-integrated (gray) numerical models under the assumption that the entire observed luminosity is due to the release of the heat deposited in the external surface layers. They also assumed that heat is deposited uniformly through a layer that, from the top of the atmosphere, extends down to a column density  $y_0$ , corresponding to the “characteristic stopping length” of the impinging particles;  $y_0$  is assumed to be a constant and is taken as a model parameter. In strict analogy to the approach used in the literature when investigating stationary, accreting atmospheres (see e.g. Turolla et al. 1994; Zampieri et al. 1995; Zane et al. 1998), the energy balance equation is modified into

$$\frac{\chi_p}{\chi_{sc}} \left[ \frac{aT^4}{2} - \frac{\chi_p^{(1)} U^{(1)}}{\chi_p} - \frac{\chi_p^{(2)} U^{(2)}}{\chi_p} \right] + (\Gamma - \Lambda)_C = \frac{W_H}{c\chi_{sc}}, \quad (2)$$

where  $(\Gamma - \Lambda)_C$  is the Compton heating-cooling term, the inclusion of which is necessary to ensure the energy balance in the external layers. In the above expression  $\chi_{sc}$  is the mean scattering opacity and  $W_H$  can be approximated by

$$W_H = \begin{cases} \frac{L_\infty}{4\pi R^2 y_0} & y < y_0 \\ 0 & y \geq y_0 \end{cases}, \quad (3)$$

where  $L_\infty$  is the luminosity observed at infinity and  $R$  is the star

radius. The local luminosity at the atmosphere surface is

$$L = L_\infty \left(1 - \frac{2GM}{Rc^2}\right)^{-1}, \quad (4)$$

where  $M$  is the neutron star mass. The main problem is then the calculation of the characteristic stopping length. [González-Caniulef et al. \(2019\)](#) describes in detail the chain of processes that are expected to contribute to the particle deceleration. Briefly summarised, impinging particles travel along the magnetic field lines, scatter and can release a photon. The process is then repeated through a new scattering until complete deceleration of the primary particle. The released photons can trigger an electron-positron avalanche and the energetic secondary particles that are produced heat the layers as they propagate further through the atmosphere.

These processes, alongside Compton drag, affect the value of the “stopping length”. It is worth noting that what we refer to as the “stopping length” is not merely the stopping length of the impacting particle; instead it refers to the length over which the heat is deposited in the atmosphere due to the chain of processes described above. These mechanisms have been discussed in detail by [González-Caniulef et al. \(2019\)](#), who produced numerical simulations and concluded that, for impinging particles with Lorentz factor  $\gamma = 10^3$ , the characteristic stopping column density is in the range  $y_0 \approx 65\text{--}500 \text{ g cm}^{-2}$ . Figure 1 shows the temperature profile of atmospheres experiencing particle bombardment as a function of the column density, as computed by [González-Caniulef et al. \(2019\)](#); the model parameters are listed in Table 1.

A hot layer is formed at the surface of the atmosphere where free-free cooling is not sufficient to radiate the heat released by particle bombardment and thermal equilibrium is instead maintained by Compton cooling. This hot external layer extends until the density is large enough for free-free cooling to kick in ([Zane et al. 2000](#); [González-Caniulef et al. 2019](#)). It is worth noting that the extension of this layer does not correspond to the stopping column density  $y_0$ .

As it can be seen, varying  $B$  results in no significant change to the temperature profile (see models 9, 10 and 11 in Figure 1). On the other hand, by increasing  $L_\infty$  the hot external layer (where the heat deposited in the bombardment process is dissipated by Compton cooling) extends deeper into the atmosphere, producing higher temperatures (models 1 and 2 in Figure 1). Also, the external layer becomes hotter and wider by decreasing  $y_0$  (see again Figure 1, models 5 and 6). The most striking feature, common to all cases, is however the presence of a nearly flat temperature profile in an extended zone of the atmosphere.

In a more realistic scenario, irradiation from the underlying crust can also contribute to the emitted luminosity, as is the case of a passive atmosphere. As a consequence, one qualitatively expects that at some depth inside the atmosphere the temperature will start raising inward in response to the heat flowing from the crust. Figure 2 shows the temperature profile of a standard cooling atmosphere, self-consistently calculated with the numerical code by [Lloyd \(2003\)](#) for  $B = 3 \times 10^{14} \text{ G}$  and  $L_\infty = 10^{36} \text{ erg s}^{-1}$ , together with a bombarded model with the same  $B$  and  $L_\infty$  (model 1 in Figure 1). A possible profile for a bombarded atmosphere heated also from below is shown by the cyan line.

In a gray, unmagnetised, pure scattering atmosphere the temperature scales with depth as  $\tau^{1/4} \sim y^{1/4}$ . On the wake of these considerations, we adopt a simplified approach in which the inner temperature profile is a power-law with index  $\alpha$  ranging from 0.05 to 0.25 and starting at different atmospheric depths  $y_*$ . Clearly, this is an oversimplification and is just useful for illustrative purposes. It has been also speculated that particle bombardment can produce an “inverted

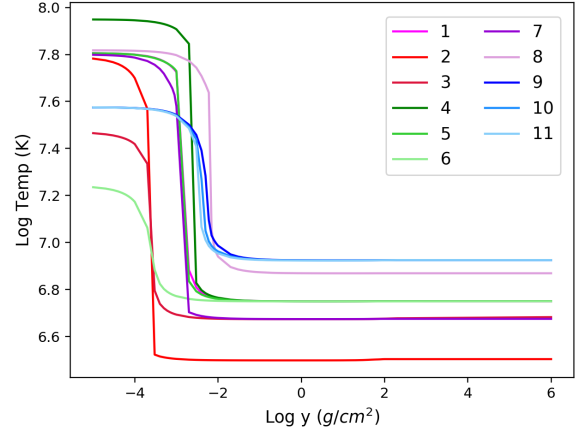


**Figure 1.** Temperature as a function of column density for atmospheres experiencing particle bombardment for different magnetic field strengths  $B$ , luminosities  $L_\infty$  and stopping column densities  $y_0$ . The parameters values for the different models are reported in Table 1.

**Table 1.** Parameter values for the models displayed in Figure 1.

Model	$B$ (G)	$L_\infty$ (erg s $^{-1}$ )	$y_0$ (g cm $^{-2}$ )
1	$3 \times 10^{14}$	$10^{36}$	100
2	$3 \times 10^{14}$	$10^{35}$	100
3	$4 \times 10^{14}$	$10^{35}$	200
4	$4 \times 10^{14}$	$10^{36}$	70
5	$4 \times 10^{14}$	$10^{36}$	100
6	$4 \times 10^{14}$	$10^{36}$	500
7	$3 \times 10^{14}$	$5 \times 10^{35}$	100
8	$3 \times 10^{14}$	$3 \times 10^{36}$	100
9	$3 \times 10^{14}$	$5 \times 10^{36}$	200
10	$6 \times 10^{14}$	$5 \times 10^{36}$	200
11	$8 \times 10^{14}$	$5 \times 10^{36}$	200

temperature profile”, with the temperature decreasing inward in some layers, and that this may be responsible for an excess of O-mode photons in the emitted radiation ([González-Caniulef et al. 2019](#); [Taverna et al. 2022](#)). In order to investigate this, we also consider slightly negative slopes. The set of temperature models used in our calculations is shown in Figure 3. The models are labelled in terms of ‘equivalent isotropic luminosity’ for visualisation purposes. This value is the model flux multiplied by  $4\pi R^2$  and hence each curve can be re-scaled once a fraction of the emitting area is specified.

## 2.2 Model regime

Our model relies on the standard twisted magnetosphere regime detailed in [Beloborodov & Thompson \(2007\)](#); [Beloborodov \(2013\)](#). In this scenario, as is described in [Beloborodov & Thompson \(2007\)](#), the current needed to circulate around the magnetic field lines and

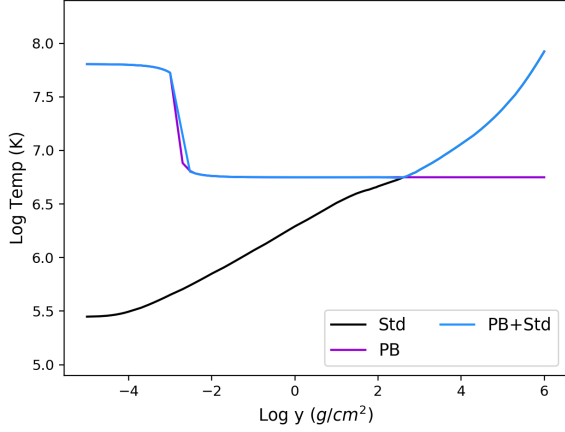


**Figure 2.** Temperature as a function of atmospheric column density for a bombarded atmosphere (purple curve) and a standard cooling atmosphere (black curve). The cyan line shows a tentative profile for a bombarded atmosphere heated also from below. Here,  $B = 3 \times 10^{14}$  G,  $L_\infty = 10^{36}$  erg/s and  $\gamma_0 = 100$  g/cm<sup>2</sup>

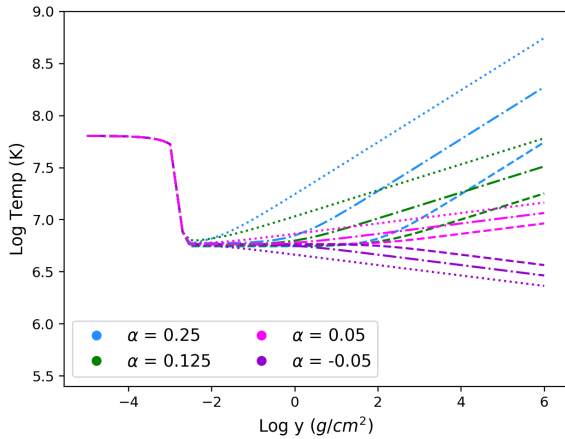


**Figure 3.** Temperature profiles for different choices of the power-law slope  $\alpha = 0.25, 0.125, 0.05, -0.05$  and matching depth  $\log \gamma_* = -2, 0, 2$  (dotted, dash-dotted, and dashed lines, respectively); here the external hot layer is taken from model 1 in Figure 1.

sustain the twist cannot be carried by electrons/protons only. Would that be the case, the solution would be described by a “relativistic double layer” (the simple circuitual analogue of a twisted, current-carrying bundle) in which the potential drop required to produce the conduction current is huge ( $\Phi_{PD} \sim 10^6$  GeV) and electrons are accelerated up to  $\gamma \sim 10^3$ . In this case, the twist would decay immediately. Instead, the reason a twist can be sustained is entirely due to the presence of pairs.

Surface thermal photons with energy  $\epsilon$  resonantly scatter onto electrons when

$$\frac{\epsilon}{m_e c^2} \frac{\gamma}{1 - \beta \cos \theta} = \frac{B}{B_Q}, \quad (5)$$

where  $B_Q = 4.413 \times 10^{13}$  G is the quantum critical field,  $\beta = v/c$  is the charge velocity (in units of the speed of light) along the magnetic field and  $\theta$  is the angle between the photon direction and the magnetic field. In the inner magnetospheric region around a magnetar, where  $B > 2B_Q$ , 1 keV photons (typically emitted by the neutron star surface) scatter onto  $\gamma > 1000$  electrons. The scattered photons have energy  $\epsilon'$  in the MeV range and initially propagate along the magnetic field. However, as soon as the photon trajectory deviates from the field line by a finite angle  $\theta$ , the condition

$$\epsilon' > \frac{2m_e c^2}{\sin \theta} \quad (6)$$

can be satisfied and the photons convert into pairs via

$$\gamma + B = e^+ + e^- + B. \quad (7)$$

Pair production along the entire circuit efficiently screens the potential and the “twist bundle” current  $j_B$  can then be conducted with  $\Phi \ll \Phi_{DL}$ . As discussed in these papers (see also Beloborodov & Thompson 2007; Beloborodov 2013; Zane et al. 2011; Turolla et al. 2015), a quasi-stationary state develops in which the particle energy has just the value required to ignite the pair cascade. For scattering onto soft X-ray photons ( $\sim 1$  keV) this is  $\gamma \sim 1000$ .

As is shown by Beloborodov (2013), at larger distance from the star surface repeated scatterings can slow down the pairs, thus above a few neutron star radii the circuit contains mildly relativistic charges ( $\gamma \sim 10$ ). It is nonetheless understood that before being able to create pairs in the inner region, electrons must reach  $\gamma > 1000$ , and so the parts of the twist bundle closer to the surface of the neutron star are populated by electrons (and positrons) with a Lorentz factor of that order. For our work we assume bombardment by a population of single velocity charges from close to the surface.

### 2.3 Radiative transfer

To calculate the emergent X-ray spectrum and polarisation degree we use the numerical code described in Lloyd (2003), with some modifications to deal with the case at hand. In particular, we turned off the self-consistent calculation of the temperature profile, so that the latter can be fed in input according to the prescription discussed in the previous section. The radiative transfer equations

$$\mu \frac{dI_V^j(\mathbf{k})}{\rho dz} = \chi_V^j(\mathbf{k}) I_V^j(\mathbf{k}) - \eta_V^j(\mathbf{k}), \quad (8)$$

are then solved for the two polarisation modes, assuming a geometrically thin plane-parallel atmosphere composed of fully-ionised hydrogen. Here,  $\mu = \cos \theta_k$ , where  $\theta_k$  represents the angle the ray makes with the slab normal, the photon momentum  $\mathbf{k}$  is described by  $\mu$  and the azimuthal angle  $\phi$ ,  $I_V^j$  is the monochromatic intensity for mode  $j$ , and  $\chi_V^j(\mathbf{k})$  and  $\eta_V^j(\mathbf{k})$  are the monochromatic opacity and emissivity respectively. Thomson scattering and bremsstrahlung emission/absorption are accounted for, while mode conversion at the vacuum resonance is neglected for simplicity. An iterative method is then used to calculate the scattering integrals (see Lloyd 2003, for all details).

We use a grid of 100 depth and 15  $\mu$  points, and, at this stage, we compute models with an aligned magnetic field (so that the azimuthal angle becomes unnecessary). Our models are computed assuming a star mass  $M = 1.4 M_\odot$  and radius  $R = 10$  km, equating to a surface gravity  $g = 2.4 \times 10^{14}$  cm/s<sup>2</sup><sup>1</sup>.

<sup>1</sup> The original bombarded temperature profiles (see Section 2.1) were com-

Once the emergent intensity and its moments are computed, for the two modes of polarisation, we calculate the intrinsic polarisation degree of the emitted radiation, defined as

$$PD_{\text{em}} = \frac{J_{\nu}^{\text{X}} - J_{\nu}^{\text{O}}}{J_{\nu}^{\text{X}} + J_{\nu}^{\text{O}}}, \quad (9)$$

where  $J_{\nu}^{\text{X(O)}} \equiv J_{\nu}^{\text{X(O)}}|_{y=0}$  is the emergent mean monochromatic intensity of X (O) mode photons, such that positive  $PD_{\text{em}}$  indicates X-mode dominated emission.

### 3 RESULTS

In this section, we investigate how particle bombardment and different heating contributions from the crust affect the polarisation properties of the radiation emerging from a single slab of magnetar atmosphere.

Figure 4 shows the mean intensity spectra as a function of energy for the three temperature profiles presented in Figure 2. At variance with the case of a standard cooling atmosphere, panel (b), the spectrum from a bombarded model, panel (a), is more blackbody-like, the contributions of the two modes are closer and the proton cyclotron line (which for these parameters is at about 2 keV) is not visible. These features are a direct consequence of the presence of an extended temperature plateau in the bombarded atmosphere (see again Figure 2). Since the X-mode opacity is much reduced with respect to that of the O-mode, X-mode photons decouple deeper in the layer and carry the imprint of the temperature there. If  $T$  increases with depth (as in the standard cooling atmosphere), this results in a dominance of X-mode photons, which come from hotter regions, especially at higher energies where the free-free opacity drops. On the other hand, if the temperature is constant, X- and O-mode photons still come from different depths, but their spectra are much closer to each other (and closer to the same blackbody). The lack of the proton cyclotron feature in panel (a) can be explained likewise. The huge opacity at the resonance forces X-mode photons back to thermal equilibrium, so that their spectrum approaches that of the O-mode. The appearance of a noticeable absorption feature is then related to how far apart the X- and O-mode continua are near the resonance. The spectrum for the combined temperature profile, panel (c), clearly exhibits intermediate properties among the two extreme cases discussed above. The cyclotron line is still present, albeit much reduced, and the X-mode dominates above  $\sim 2$  keV because photons of these energies come from the hotter regions, where  $T$  increases inward.

The energy-dependent polarisation degree for the three models discussed above is shown in Figure 5. As expected from our previous considerations, emission from particle bombardment is polarised in the X-mode but the polarisation degree is significantly lower ( $\sim 25\%$ ) than in a standard cooling atmosphere (almost 100%). The model with combined temperature profile results in a signal with intermediate properties. The polarisation degree exhibits the characteristics of the bombarded model for energies below  $\sim 0.2$  keV after which it raises until it attains  $\sim 100\%$  at  $\sim 5$  keV. The drop in polarisation around  $\sim 2$  keV reflects the absorption of X-mode photons at the proton cyclotron resonance. This is much more pronounced than in the passively cooling model because of the different X-to-O ratio (see also panels b and c in Figure 4).

puted using  $M = 1 M_{\odot}$  as in González-Caniulef et al. (2019). We checked that using  $M = 1 M_{\odot}$  produces only marginal changes in our polarisation results ( $\leq 2\%$ )

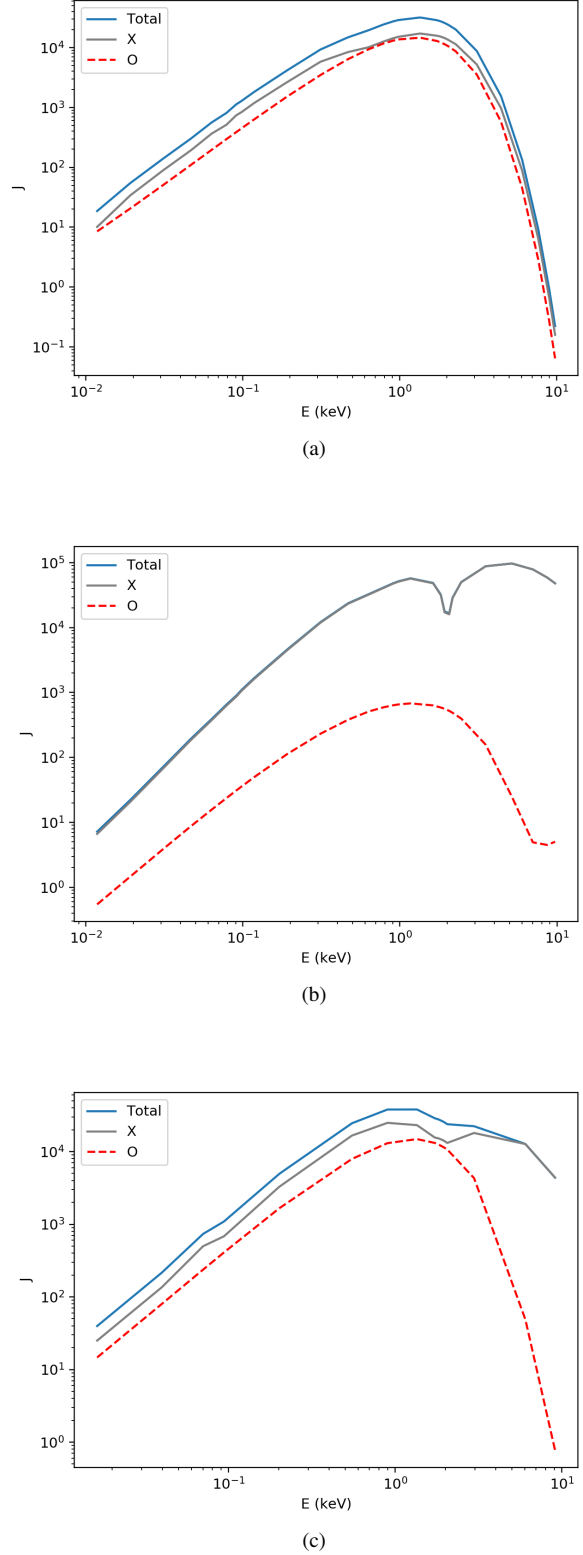


**Figure 4.** Mean intensity (in  $\text{erg cm}^{-2} \text{s}^{-1} \text{keV}^{-1}$ ) spectrum of the emergent radiation as a function of the photon energy  $E$  for the three cases described in Figure 2, where (a) is the bombarded profile, (b) is the standard cooling atmosphere and (c) is the bombarded atmosphere also heated from the crust.

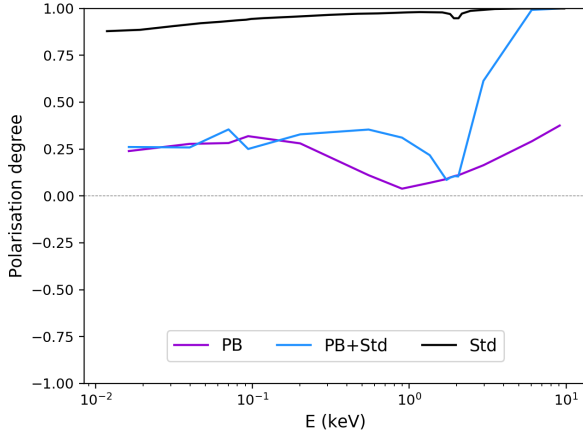


**Figure 5.** Polarisation degree as a function of the photon energy  $E$  for the models shown in Figure 2.

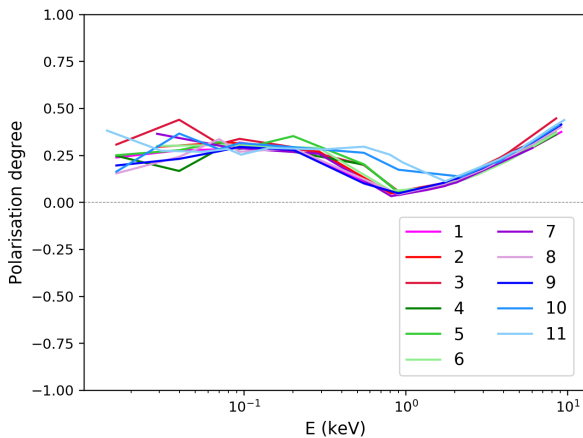


**Figure 6.** Polarisation degree as a function of photon energy  $E$  for atmospheres experiencing particle bombardment with temperature profiles shown in Figure 1.

We address next the polarisation properties of the bombarded atmosphere models for all the temperature profiles presented in Figure 1, which cover different magnetic field strengths  $B$ , luminosities  $L_\infty$  and stopping column densities  $y_0$  (see also Table 1). The corresponding polarisation degree, as a function of the photon energy, is shown in Figure 6. As it can be seen, all models essentially follow the qualitative behaviour exhibited by model 1 which is actually the one we presented in Figure 5. The largest departures are for the most magnetised cases (models 10 and 11) which show a somewhat higher polarisation around 1 keV.

To explore this issue further, we considered the set of (ad hoc) temperature profiles discussed in Section 2.1, computed by assuming a particle bombardment profile for  $B = 3 \times 10^{14}$  G,  $L_\infty = 10^{36}$  erg/s and  $y_0 = 100$  g/cm<sup>2</sup> (model 1 in Table 1) in the external region below a given column density  $y_*$ , and a power-law profile, with index  $\alpha$ , for  $y \geq y_*$  (see Figure 3). In order to investigate the effects of an

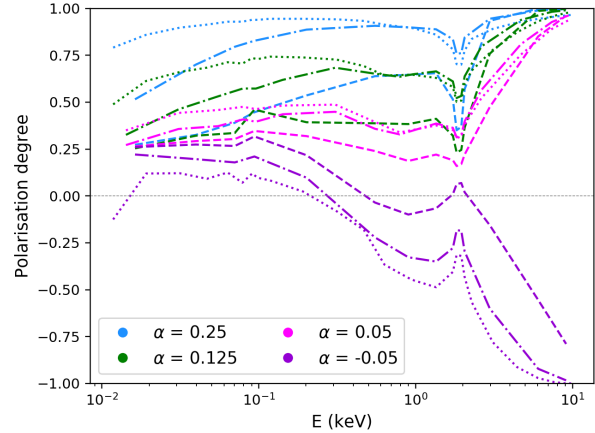


**Figure 7.** Polarisation degree as a function of the photon energy  $E$  for atmospheres experiencing particle bombardment with the temperature profiles shown in Figure 3 (line code is the same here).

“inverted temperature profile”, we also considered a power-law with slightly negative slopes.

The results of our radiative transfer calculation are shown in Figure 7 for different values of  $y_*$  and  $\alpha$ . If the temperature profile at some point starts increasing with depth, as expected in the presence of crustal heating, the emergent signal is always dominated by the X-mode at all frequencies. Models in which the temperature starts increasing at a lower depth, closer to the top of the atmosphere and to the Compton-cooled bombarded layers, have larger polarisation degrees in the lower energy range ( $< 1$  keV) when compared with models with the same value of  $\alpha$  but larger  $y_*$ . Steeper slopes also results in a polarisation degree which increases more rapidly with energy. However, in all cases we considered, if the internal temperature profile increases inward (positive  $\alpha$ ) the emergent signal tends to be polarised 100% in the X-mode at 10 keV. In contrast, if for some reasons the temperature profile decreases towards the base of the atmosphere, then a change in the dominant polarisation mode occurs, with an emergent signal that becomes O-mode dominated at high energies.

Motivated by this, as a final test, we considered models in which the external layers ( $y \leq 10^{-3}$  g cm<sup>-2</sup>) are still assumed to be heated by particle bombardment (model 1 is assumed in the following), but the temperature profile follows a broken power law as  $y$  increases. The first power law component decreases with depth and extends in an intermediate layer, while the second one increases inward and is applied to the innermost regions. For the increasing leg we considered the reference slope  $\alpha_2 = 1/4$  of the gray, passive cooling atmosphere, and a case with half this value. For the decreasing part we investigated cases with a slightly decreasing behaviour ( $\alpha_1 = -0.05, -0.1$ , so to mimic a small deviation from the completely flat profiles of Figure 1) and two more extreme, albeit unphysical, cases with  $\alpha_1 = -1/4, -1/8$ . We also explored the effect of varying the extension of the two regions. The temperature profiles are illustrated in Figure 8(a) and the results of the radiative transfer calculation are shown in Figure 8(b).

For models with  $\alpha_1 \leq 0.1$  (blue and green curves in Figure 8), the emergent signal is dominated by the X-mode in almost the entire energy range, with the exception of the very low energies below  $\sim 3 \times 10^{-2}$  keV and, possibly, of the region near the proton cyclotron

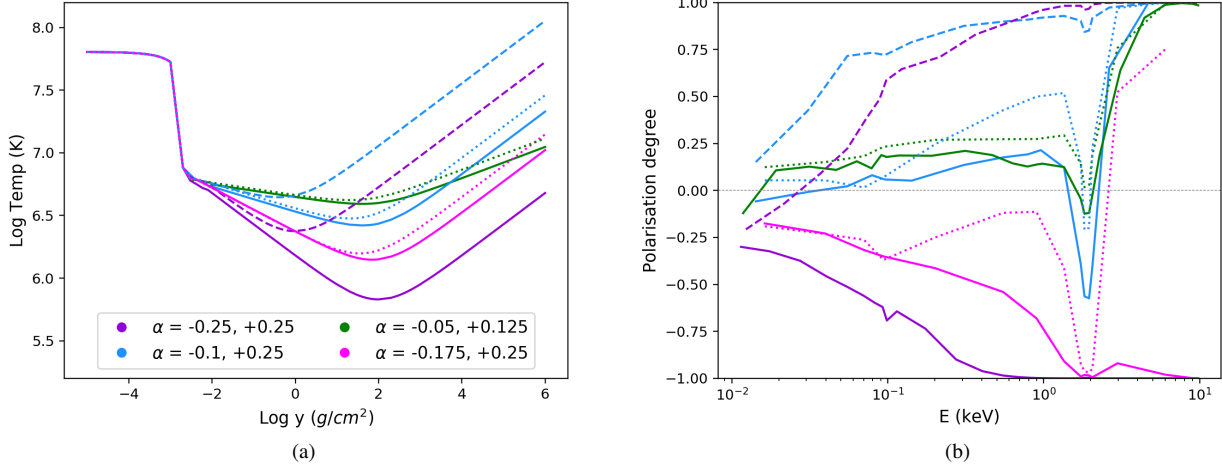


**Figure 8.** Temperature (a) and polarisation degree (b) for atmospheres experiencing particle bombardment in the most external layer (same model used in Figure 3), but with a double power law temperature profile. The temperature is first assumed to decrease with index  $\alpha_1 = -0.25, -0.175, -0.1, -0.05$ , starting from a depth  $\log y_1 = -2$  and then to increase with index  $\alpha_2 = 0.25, 0.125$  starting from a depth  $\log y_2 = 2$  (solid lines),  $\log y_2 = 1.7$  (dotted lines) and  $\log y_2 = 0$  (dashed lines).

energy. This is also true for all models in which the temperature starts rising at a lower depth (i.e.  $\log y_2 = 0$ ). The polarisation degree increases with energy (apart from the depolarisation which appears near the cyclotron energy). Higher temperatures deeper in the atmosphere result in higher polarisation degrees across the whole energy range. The proton cyclotron line is present in all spectra. In order to produce an O-dominated signal in a wide energy band, a very steep inverted temperature profile, extending up to the entire stopping length (i.e.  $y_2 = y_0 = 100 \text{ g/cm}^2$ ) is required, as shown by the purple and magenta solid lines in Figure 8. We have only produced one scenario, when the knee in the broken temperature power-law occurs at  $\log y = 1.7$  (magenta dotted curve in Figure 8) where the emission switches from O- to X-mode dominated close to the *IXPE* energy range (2–8 keV). The dominance switch from O-mode to X-mode can be seen around the cyclotron energy. However, for this switch to occur in and around the *IXPE* energy range a very steep inverted slope is necessary, and this is therefore an unrealistic model.

#### 4 APPLICATION TO SOURCES

In order to compare our results with the recent observations of magnetars performed by *IXPE*, we need to compute the model spectropolarimetric properties as seen by a distant observer. To this aim, we use a ray-tracing technique which sums together the contributions from the parts of the star surface which are in view at each rotational phase (Zane & Turolla 2006, see also Taverna et al. 2015; González Caniulef et al. 2016). In doing this, we first compute the monochromatic, phase-dependent flux of the three Stokes parameters  $I, U, Q$  and then calculate the observed flux, polarisation degree,  $\sqrt{Q^2 + U^2}/I$ , and angle,  $\arctan(U/Q)/2$ , at each rotational phase. We assume a core-centred dipole magnetic field and include general relativistic corrections.

We first address the question of whether particle bombardment can be a viable explanation for the modest polarisation observed from these sources at low energy, in alternative to condensed surface emis-

sion, as suggested by Taverna et al. (2022) and Zane et al. (2023). We assume two different geometries for the bombarded atmospheric patch: a polar cap with semi-aperture of  $5^\circ$ , and an equatorial region with semi-aperture of  $5^\circ$  in both latitude and azimuth. This is motivated by the fact that similar geometries have been invoked to explain the polarisation at low energies measured by *IXPE* in 4U 0142+61 and 1RXS J1708 (Taverna et al. 2022; Zane et al. 2023). In both cases, we divided the surface region into two patches in co-latitude, such that the magnetic field inclination in each patch is  $\theta_B = (0^\circ, 5^\circ)$  and  $(85^\circ, 89^\circ)$  for the cap and the equatorial spot, respectively. Radiative transfer models have been computed by accounting for the inclination of the magnetic field, which introduces an azimuthal dependence in the radiation field. For the calculation, we used the same grids as in the previous section, and in addition an azimuthal mesh with 5 points such that the ray direction and magnetic field is calculated for each  $(\mu, \phi)$  pair (see Lloyd 2003, Section 4.2.2, for more details). Here we discuss the limiting case in which the emission is produced only by the particle bombardment, since this is the scenario in which we expect the emergent signal to have a suitably low polarisation degree. We used model 1<sup>2</sup> from Table 1, with  $B = 3 \times 10^{14} \text{ G}$ ,  $L_\infty = 10^{36} \text{ erg/s}$  and  $y_0 = 100 \text{ g/cm}^2$ . For the rest of the surface, we assumed unpolarised blackbody emission at a very low temperature such that the contribution to the total spectrum is negligible.

Figure 9 shows the phase-averaged polarisation degree, in the 2–3 keV energy range, as seen by a distant observer, as a function of the angles that the spin axis makes with the line-of-sight,  $\chi$ , and the magnetic axis,  $\xi$ , respectively. We find that the maximum observed polarisation degree is  $\sim 25\%$  in the polar cap model (Figure 9a), while it is slightly lower for the equatorial spot (Figure 9b). Both of these are compatible with the polarisation properties observed from 1RXS J1708 in the same energy range. Emission from a hot spot heated by particle bombardment could therefore explain *IXPE* measurement at low energies.

<sup>2</sup> The models have been computed in terms of observed effective temperature. The luminosity is then correctly associated to each surface patch accounting for the corresponding patch area.

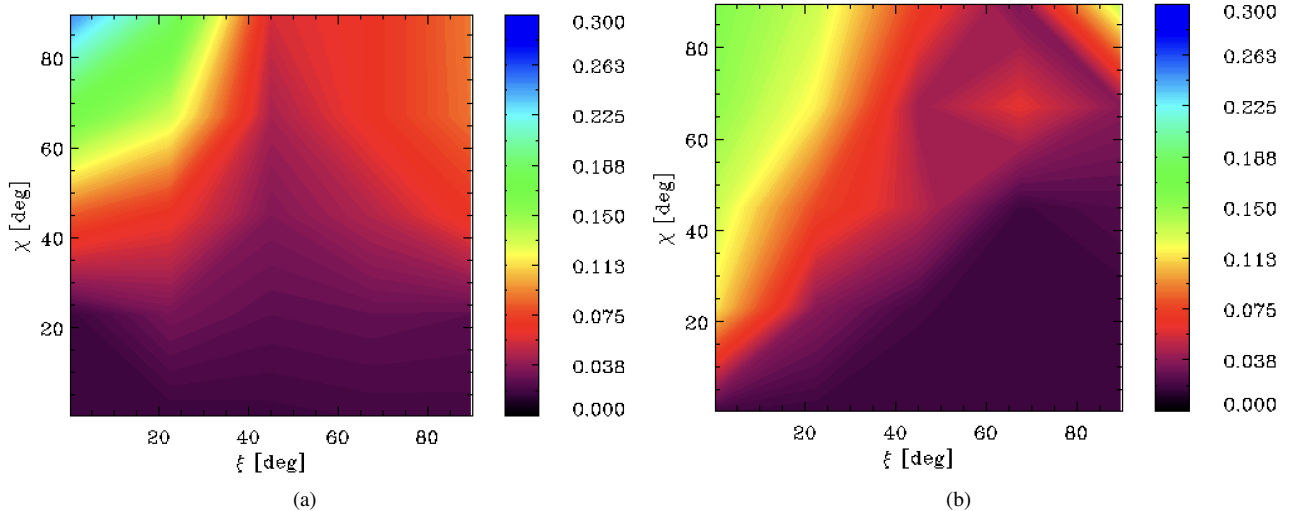


**Figure 9.** The phase-averaged polarisation degree in the 2–3 keV energy range as function of the two angles  $\chi$  and  $\xi$  for a bombarded atmosphere on top a polar cap (a) and an equatorial patch (b). See text for model details.

Additionally, the polarisation degree observed from 4U 0142+61 could potentially agree with our models. The  $90^\circ$  rotation in polarisation angle between the low and high energy ranges cannot be accommodated in this scenario alone. However, including RCS (as proposed by Taverna et al. 2022), particle bombardment certainly cannot be ruled out as an explanation for this magnetar either. We have not produced models of the emission at infinity for the case from Figure 8 in which the polarisation goes from O-mode dominated to X-mode dominated at  $\sim 3$  keV (magenta dotted curve) because for this to occur an unrealistically, unphysically large decrease in temperature would be needed and we have no astrophysical reason to believe that this would ever occur.

## 5 DISCUSSION AND CONCLUSIONS

In this work we have investigated the polarisation properties from magnetar atmospheres experiencing particle bombardment. We computed simplified models using ad-hoc assumptions on the temperature profile, mimicking scenarios in which the emission is powered by different combinations of particle bombardment and heat injection from the crust. We also considered extreme cases in which some internal atmospheric layers are characterised by a smooth, inverted thermal profile that slightly decreases inward. We have found that particle bombardment can, in principle, produce a distinct polarisation signature.

When assuming that the luminosity is only due to the release of heat from particle bombardment, with no significant contribution from the crustal heating, we find that the magnetar X-ray emission has a polarisation degree that remains around 20% below  $\approx 0.2$  keV, dips slightly and then increases  $\approx 5$ –40% between 1–10 keV. The emission is X-mode dominated.

Unsurprisingly, when the contribution to the total luminosity from crustal heating is increased, polarisation properties tend towards those of a standard cooling atmosphere. Atmospheres that exhibit a steeper increase in temperature in the internal layer produce radiation with higher polarisation degrees, while moving inward the depth at which the temperature starts to increase results in a less polarised signal. Additionally, inverted profiles, in which the temperature decreases with depth, may in principle result in O-mode dominated

emission in the X-ray band, although the required slope appears to be unphysically large. However, in the case of particle bombardment onto a non-magnetised atmosphere, it has been found that particles with low Lorentz factor ( $\gamma \sim 10$ ) bombarding the atmosphere can produce heat deposition in a very shallow layer and give rise to an inner region with a relatively steep inverted temperature slope (Bauböck et al. 2019). This study is not directly applicable to the regime we are using in this work, among other reasons because in our study we account for the fact that the length within which heat is deposited is larger than the stopping length of primary charges (see section 2.1). An in-depth study and proper calculation therefore need to be carried out to investigate if a similar scenario could be possible in the magnetised plasma of a magnetar atmosphere and if these seemingly unphysical temperature slopes, required for an O-mode dominated spectrum, can in fact be produced.

Particle bombardment alone cannot fully explain the polarisation features observed by *IXPE* in magnetar sources. However, a bombarded atmosphere combined with other emission models (like a standard atmosphere, RCS, a condensed surface, etc.) may provide a viable explanation for the polarisation pattern detected at low energies. Specifically, in the case of 1RXS J1708, particle bombardment is in agreement with the emission in the 2–3 keV range. We speculate that a hot spot heated by particle bombardment coupled with standard atmospheric emission would be a likely scenario, as proposed by Zane et al. (2023), as an alternative to the one based on a combination of gaseous and condensed components. Additionally, models that combine particle bombardment and magnetospheric RCS could also potentially explain the emission from both 4U 0142+61 and SGR 1806–20. Testing these combined models is outside the scope of this current paper but is an exciting prospect for future work.

It is predicted that the external magnetic fields of magnetars are complex and contain local twists, with particle bombardment taking place only in a small selection of magnetic colatitudes. However, the implementation of a more complex field structure is not achievable for this work. Instead, we produce the emission at infinity assuming a global dipolar field in our ray-tracing simulation and allow contributions to the emission spectrum from only small patches of the surface. While this simplification of the magnetic structure will likely have an impact on the polarisation spectrum, the global twist is



a well-known and commonly used approximation (see e.g. Thompson et al. 2002; Fernández & Davis 2011; Taverna et al. 2014). The development of a model including complex magnetic field structures and the investigation of the magnetic field evolution are important areas of ongoing and future works.

In principle, to fully probe the effects of particle bombardment the full thermal and pressure structure of the atmosphere should be solved coupled with radiative transfer, relaxing the assumptions of radiative and hydrostatic equilibrium. Additionally, our models assume a fully-ionised hydrogen plasma and do not include vacuum contributions to the plasma dielectric tensor. Vacuum birefringence and mode conversion effects can significantly affect the polarisation properties of the emission around and above the quantum critical field (Zane et al. 2000; Ozel 2001; Ho & Lai 2003; Ho et al. 2003; Lai & Ho 2003; Kelly et al. 2024). The focus of this paper was to explore the potential polarisation signatures from particle bombardment on the atmosphere and further developments will be matter of future investigations.

## ACKNOWLEDGEMENTS

RK acknowledges support from The Science and Technology Facilities Council (STFC) for a PhD studentship. RTa and RTu acknowledge financial support from the Italian MUR through the grant PRIN 2022LWPEXW. DGC acknowledges support from a CNES fellowship. We would like to thank the anonymous referee for their insightful comments and helpful suggestions.

## DATA AVAILABILITY

The simulated data produced in this investigation are available on request.

## REFERENCES

- Adler S. L., 1971, *Annals of Physics*, 67, 599  
 Bauböck M., Psaltis D., Özel F., 2019, *The Astrophysical Journal*, 872, 162  
 Beloborodov A. M., 2013, *The Astrophysical Journal*, 777, 114  
 Beloborodov A. M., Thompson C., 2007, *The Astrophysical Journal*, 657, 967  
 Duncan R. C., Thompson C., 1992, *The Astrophysical Journal*, 392, L9  
 Fernández R., Davis S. W., 2011, *The Astrophysical Journal*, 730, 131  
 González Caniulef D., Zane S., Taverna R., Turolla R., Wu K., 2016, *Monthly Notices of the Royal Astronomical Society*, 459, 3585  
 González-Caniulef D., Zane S., Turolla R., Wu K., 2019, *Monthly Notices of the Royal Astronomical Society*, 483, 599  
 Hambaryan V., Wagner D., Schmidt J., Hohle M. M., Neuhäuser R., 2015, *Astronomische Nachrichten*, 336, 545  
 Harding A. K., Lai D., 2006, *Reports on Progress in Physics*, 69, 2631  
 Hernquist L., 1985, *Monthly Notices of the Royal Astronomical Society*, 213, 313  
 Heyl J., et al., 2024, *Monthly Notices of the Royal Astronomical Society*, 527, 12219  
 Ho W. C. G., Lai D., 2001, *Monthly Notices of the Royal Astronomical Society*, 327, 1081  
 Ho W. C. G., Lai D., 2003, *Monthly Notices of the Royal Astronomical Society*, 338, 233  
 Ho W. C. G., Lai D., Potekhin A. Y., Chabrier G., 2003, *The Astrophysical Journal*, 599, 1293  
 Kelly R. M. E., Zane S., Turolla R., Taverna R., 2024, *Monthly Notices of the Royal Astronomical Society*, 528, 3927

- Lai D., 2023, *Proceedings of the National Academy of Sciences*, 120, e2216534120  
 Lai D., Ho W. C. G., 2003, *The Astrophysical Journal*, 588, 962  
 Lloyd D. A., 2003, Model atmospheres and thermal spectra of magnetized neutron stars, doi:10.48550/ARXIV.ASTRO-PH/0303561, <https://arxiv.org/abs/astro-ph/0303561>  
 Mushtukov A. A., Suleimanov V. F., Tsygankov S. S., Portegies Zwart S., 2021, *Monthly Notices of the Royal Astronomical Society*, 503, 5193  
 Ozel F., 2001, *The Astrophysical Journal*, 563, 276  
 Pavlov G. G., Shibano Y. A., Ventura J., Zavlin V. E., 1994, *Astronomy and Astrophysics*, 289, 837  
 Pavlov G. G., Zavlin V. E., Trümper J., Neuhäuser R., 1996, *The Astrophysical Journal*, 472, L33  
 Potekhin A. Y., 2014, *Physics-Uspekhi*, 57, 735  
 Potekhin A. Y., Ho W. C. G., Chabrier G., 2017, Atmospheres and radiating surfaces of neutron stars with strong magnetic fields, <http://arxiv.org/abs/1605.01281>  
 Romani R. W., 1987, *The Astrophysical Journal*, 313, 718  
 Taverna R., Turolla R., 2024, *Galaxies*, 12, 6  
 Taverna R., Muleri F., Turolla R., Soffitta P., Fabiani S., Nobili L., 2014, *Monthly Notices of the Royal Astronomical Society*, 438, 1686  
 Taverna R., Turolla R., Gonzalez Caniulef D., Zane S., Muleri F., Soffitta P., 2015, *Monthly Notices of the Royal Astronomical Society*, 454, 3254  
 Taverna R., Turolla R., Suleimanov V., Potekhin A. Y., Zane S., 2020, *Monthly Notices of the Royal Astronomical Society*, 492, 5057  
 Taverna R., et al., 2022, *Science*, 378, 646  
 Thompson C., Duncan R. C., 1993, *The Astrophysical Journal*, 408, 194  
 Thompson C., Lyutikov M., Kulkarni S. R., 2002, *The Astrophysical Journal*, 574, 332  
 Tiengo A., et al., 2013, *Nature*, 500, 312  
 Turolla R., Zampieri L., Colpi M., Treves A., 1994, *The Astrophysical Journal*, 426, L35  
 Turolla R., Zane S., Watts A. L., 2015, *Reports on Progress in Physics*, 78, 116901  
 Turolla R., et al., 2023, *The Astrophysical Journal*, 954, 88  
 Weisskopf M. C., et al., 2022, *Journal of Astronomical Telescopes, Instruments, and Systems*, 8  
 Zampieri L., Turolla R., Zane S., Treves A., 1995, *The Astrophysical Journal*, 439, 849  
 Zane S., Turolla R., 2006, *Monthly Notices of the Royal Astronomical Society*, 366, 727  
 Zane S., Turolla R., Treves A., 1998, *The Astrophysical Journal*, 501, 258  
 Zane S., Turolla R., Treves A., 2000, *The Astrophysical Journal*, 537, 387  
 Zane S., Nobili L., Turolla R., 2011, in Torres D. F., Rea N., eds., *High-Energy Emission from Pulsars and their Systems*. Springer Berlin Heidelberg, Berlin, Heidelberg, pp 329–335, doi:10.1007/978-3-642-17251-9\_26, [https://link.springer.com/10.1007/978-3-642-17251-9\\_26](https://link.springer.com/10.1007/978-3-642-17251-9_26)  
 Zane S., et al., 2023, *The Astrophysical Journal Letters*, 944, L27

This paper has been typeset from a  $\text{\TeX}/\text{\LaTeX}$  file prepared by the author.